

Strong Coupling of Localized Surface Plasmons to Excitons in Light-Harvesting Complexes

Anna Tsargorodska,[†] Michaël L. Cartron,[‡] Cvetelin Vasilev,[‡] Goutham Kodali,[§] Olga A. Mass,^{||} Jeremy J. Baumberg,[⊥] P. Leslie Dutton,[§] C. Neil Hunter,[‡] Päivi Törmä,^{*,#} and Graham J. Leggett^{*,†}

[†]Department of Chemistry, University of Sheffield, Brook Hill, Sheffield S3 7HF, U.K.

[‡]Department of Molecular Biology and Biotechnology, University of Sheffield, Western Bank, Sheffield S10 2TN, U.K.

[§]The Johnson Research Foundation and Department of Biochemistry and Biophysics, University of Pennsylvania, Philadelphia, Pennsylvania 10104, United States

^{||}Department of Chemistry, North Carolina State University, Raleigh, North Carolina 27695, United States

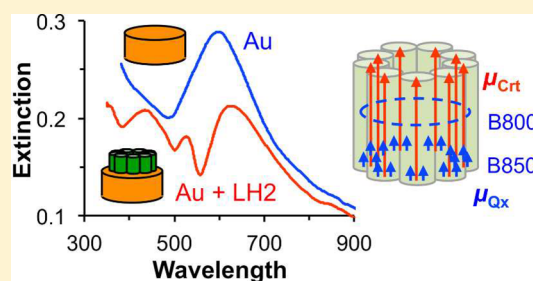
[⊥]Cavendish Laboratory, Dept. of Physics, University of Cambridge, J. J. Thomson Ave, Cambridge, CB3 0HE, U.K.

[#]COMP Centre of Excellence, Department of Applied Physics, Aalto University, School of Science, P.O. Box 15100, 00076 Aalto, Finland

Supporting Information

ABSTRACT: Gold nanostructure arrays exhibit surface plasmon resonances that split after attaching light harvesting complexes 1 and 2 (LH1 and LH2) from purple bacteria. The splitting is attributed to strong coupling between the localized surface plasmon resonances and excitons in the light-harvesting complexes. Wild-type and mutant LH1 and LH2 from *Rhodobacter sphaeroides* containing different carotenoids yield different splitting energies, demonstrating that the coupling mechanism is sensitive to the electronic states in the light harvesting complexes. Plasmon–exciton coupling models reveal different coupling strengths depending on the molecular organization and the protein coverage, consistent with strong coupling. Strong coupling was also observed for self-assembling polypeptide maquettes that contain only chlorins. However, it is not observed for monolayers of bacteriochlorophyll, indicating that strong plasmon–exciton coupling is sensitive to the specific presentation of the pigment molecules.

KEYWORDS: Strong coupling, plasmonic nanoparticles, light harvesting complexes, purple bacteria, photosynthesis



Photosynthetic organisms collect sunlight with extraordinarily high efficiencies, and the mechanisms that are responsible for this have been the subject of intense enquiry.¹ In the purple bacterium *Rhodobacter (R.) sphaeroides* sunlight is captured by light-harvesting complex 2 (LH2) and transmitted to light-harvesting complex 1 (LH1), which funnels the excitation into the photosynthetic reaction center (RC) where reduction of ubiquinone begins the process by which solar energy is converted to chemical potential energy.^{2,3} In LH2 and LH1 light energy is absorbed and transmitted via bacteriochlorophyll (BChl) and carotenoid (Crt) pigment molecules. Both molecules have cylindrical structures. LH2 consists of nine dipeptide units, with a single Crt and three BChl associated with each.¹ Two of the BChl form part of the close-packed B850 ring in which the interpigment spacing is 1 nm, and the third forms part of the B800 ring (interpigment spacing 2 nm). LH1 is slightly larger, consisting of 16 peptide units and containing 32 BChl in a single close-packed ring (the B875 ring).¹ The efficiency of light harvesting in photosynthetic antenna complexes is thought to depend strongly upon the energy sharing mechanisms in the pigment molecules.^{4,5} At close range, electron-exchange (Dexter) coupling provides

efficient energy transfer, while at longer distances, Förster hopping occurs and, at the pigment separations found in light harvesting antenna complexes,^{6,7} is expected to be efficient.⁴ Quantum mechanical calculations suggest that electronic coherence may, additionally, lead to the formation of long-lived excitons.⁸ For example, in LH2 energy migration in the B800 ring of BChl is thought to be via Förster transfer, while in the B850 ring the pigments are electronically coupled to form an exciton band, extending the lifetime of the lowest-lying excited state.⁸ Evidence from ultrafast spectroscopy has provided support for this hypothesis,^{9–14} including recent measurements on whole cells of *R. sphaeroides*, which demonstrated characteristic “quantum beats”.¹⁵

Plasmonic materials^{16,17} are nanostructured noble metal systems in which coupling between incident electromagnetic radiation and collective oscillations of surface electrons dominates optical properties yielding new phenomena.^{18–26}

Received: June 28, 2016

Revised: September 28, 2016

Published: September 30, 2016

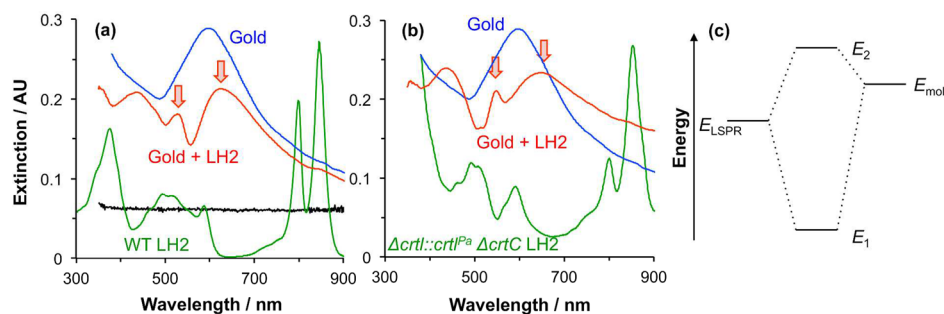


Figure 1. Extinction spectra for arrays of gold nanostructures before (blue) and after (red) attachment of (a) WT LH2 and (b) the $\Delta crtI::crtI^{Pa} \Delta crtC$ mutant of LH2. Arrows identify bands formed by splitting of the LSPR. Absorption spectra of the proteins in solution are shown in green. The black trace in (a) is the extinction spectrum of a monolayer of WT LH2 adsorbed on glass. (c) Schematic diagram illustrating the linear combination of LSPR and exciton states in strong coupling, to yield two new peaks with energies E_1 and E_2 .

They have attracted growing interest for applications in biological sensing and analysis.^{23,27–35} Recent studies have demonstrated plasmonic enhancement of fluorescence emission from light-harvesting complexes of bacteria^{36,37} and for photosystem I from chloroplasts^{38,39} via coupling between the plasmon band of a metal nanoparticle and a spectroscopic transition in the biomolecule. In the present study, a different approach is taken: changes in the extinction of metal nanostructures are measured after the attachment of light-harvesting complexes. Significantly, we have observed substantial changes in these extinctions due to strong coupling to excited states in the light harvesting complexes.

Surface plasmon polaritons (SPPs) on various nanostructures may be strongly coupled to molecular excitons that lie within the plasmon mode volume.^{40,41} A linear combination of the exciton and the uncoupled plasmon resonance yields new states above and below the energy of the SPP mode, giving rise to characteristic splittings in spectra. There has been a great deal of interest recently in such phenomena. There is a substantial body of literature on strong plasmon–exciton coupling, recently reviewed in ref 40, including studies of J-aggregates^{42–50} and dye molecules.^{51–53} Where periodic arrays of nanostructures are formed in which the period is of the order of the wavelength of the incident light, coupling of LSPRs may yield surface lattice resonances (SLRs). The coupling may be described by a modified version of Fano theory,^{54–56} or using the coupled dipole approximation.⁵⁷ SLRs too may be strongly coupled to molecular excitons that lie within the plasmon mode volume.^{52,53,58} In the present case periodic arrays are used, but their periods have been selected to be such that SLR phenomena are excluded at the wavelengths considered; instead the purpose of the array structure is, rather, to amplify the signal from single nanostructures. Here we demonstrate for the first time strong coupling of LSPRs to excitons in light-harvesting complexes from purple bacteria and to self-assembling polypeptide maquettes. The coupling energies are the range 0.08–0.21 eV and depend on both the exciton energy and the protein fractional coverage. Very different behavior is observed for films of bacteriochlorophylls alone, however, suggesting that strong coupling is very sensitive to changes in the molecular electronic structure and/or excited state lifetime.

Macroscopically extended arrays of gold nanostructures (nanodisks) were fabricated by interferometric lithography as previously described⁵⁹ (see Supporting Information for full details) and functionalized with light-harvesting complexes either by site-specific attachment to NTA-capped gold

nanostructures (LH2 and BT6 polypeptide maquettes) or by attachment to glutaraldehyde-capped surfaces (LH1).

Figure 1a (blue line) shows the extinction spectrum of a hexagonal array with period 310 ± 30 nm and nanodisks of diameter 154 ± 22 nm and height 19 ± 3 nm (an AFM image is provided in the Supporting Information). A dramatic change is observed after binding of wild-type LH2 (Figure 1a, red line): the plasmon band splits to yield new components at 527 and 624 nm (marked with arrows). In contrast, a monolayer of the protein adsorbed onto a glass slide yields none of these peaks; indeed there are no signals greater than the noise (black line in Figure 1a) because the spectrophotometer used here has limited sensitivity. The dramatic change in the extinction spectrum after attachment of LH2 to the array of gold nanostructures cannot therefore result simply from adsorption of the protein, but must instead result from plasmon–protein coupling. There is a large literature on plasmonic detection of proteins, but previously published work reports only a red shift in the plasmon band after adsorption of protein.²³ To illustrate this, we have included in the Supporting Information an extinction spectrum recorded for exactly the same array of gold nanostructures used in Figure 1 after attachment of green fluorescent protein. There is no evidence of splitting, and instead a small red shift is observed in the position of the plasmon band. We hypothesize that the changes in Figure 1b result from strong coupling between the protein and the LSPR, as further evidenced below.

The carotenoid in wild-type (WT) LH2 is spheroidenone, so the experiment was repeated using a $\Delta crtI::crtI^{Pa} \Delta crtC$ mutant, in which the carotenoid is instead predominantly lycopene. Apart from the changed *Crt*, the structure of the protein is identical to that of WT LH2. The same array was used (after careful cleaning in piranha solution, such that the extinction spectrum of the clean array was unchanged). After attachment of the mutant protein, splitting is observed, but now peaks are observed at 547 and 649 nm, i.e. red-shifted compared to WT LH2 (arrows in Figure 1b).

In the strong coupling regime, a linear combination of a protein exciton (energy E_{mol}) and the uncoupled LSPR (energy E_{LSPR}) yields new states above and below the energy of the LSPR, with energies E_1 and E_2 , giving rise to splitting of the main plasmon resonance (Figure 1c). The behavior observed in Figure 1a,b is consistent with this. Although the Q_x band (peak at 588 nm, 2.11 eV in the solution phase spectra, green lines, in Figures 1 and 2) is closest to the plasmon resonance of the clean gold, the significant differences between the extinction spectra acquired after attachment of the two different LH2

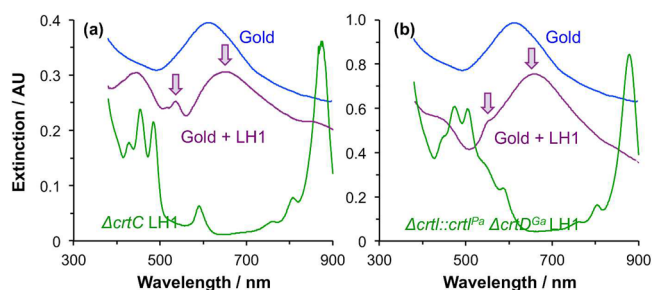


Figure 2. Extinction spectra for arrays of gold nanostructures before (blue) and after (purple) attachment of (a) the $\Delta crtC$ mutant of LH1 and (b) the $\Delta crtI::crtI^{Pa} \Delta crtD^{Ga}$ mutant of LH1. Absorption spectra of the proteins in solution are shown in green.

proteins is evidence that the LSPR couples to a transition in the Crt as well as, or instead of, the Q_x transition. Among the Crt exciton transitions, the S2 is nearest in energy to the LSPR. In each of the solution-phase spectra (green lines) in Figure 1, a cluster of three peaks (around 500 nm) is in fact observed corresponding to the S2 transition. These are due to vibronic coupling, and the lowest energy transition in each case is the 0–0 line, which corresponds to a transition in a Crt in the vibrational ground state. The energies of these transitions are reported as 562 nm, 2.21 eV for spheroidenone in LH2⁶⁰ and 539 nm,⁶¹ 2.30 eV for lycopene.⁶¹

A strong extinction is also observed at 435 nm in Figure 1a after attachment of LH2 to the gold nanostructures. A peak was sometimes observed at this wavelength for clean gold, albeit at much reduced intensity, and its position was invariant with the identity of the protein. Its origin is unclear, but it appears to be

unrelated to the splitting observed between 500 and 700 nm in the spectra in Figure 1.

Similar observations were made when the behavior was compared for two mutants of LH1 with different Crt compositions (but otherwise identical structures). For a clean gold array the LSPR was at 613 nm (blue trace in Figure 2a,b). After attachment of the $\Delta crtC$ mutant of LH1, in which the Crt is neurosporene,⁶² splitting of the plasmon band is observed (Figure 2a), yielding components at 537 and 652 nm. The array was cleaned and the experiment repeated, but this time with the $\Delta crtI::crtI^{Pa} \Delta crtD^{Ga}$ mutant. This mutant contains several carotenoids.⁶² The most abundant components are lycopene and rhodopsin. Splitting is again observed, but this time the features are less pronounced (Figure 2b). Neurosporene yields peaks at higher energy in the $\Delta crtC$ mutant than do the carotenoids that are present in the $\Delta crtI::crtI^{Pa} \Delta crtD^{Ga}$ mutant, which possibly explains the reduced splitting observed after attachment of the protein in Figure 2b.

The adsorption isotherm for WT LH2 on NTA-terminated gold nanostructures was determined (see Supporting Information) and the extinction spectra measured as a function of the fractional coverage of the protein, θ (Figure 3a). For low concentrations of protein in solution, the absorption spectra exhibited lower signal/noise making quantification difficult; consequently fractional coverages below 0.59 were not studied. However, significant changes were observed in the extinction spectra for $0.59 < \theta < 0.97$. For $\theta = 0.97$, two components at 2.21 and 2.38 eV are well resolved. As θ is reduced toward 0.81, the splitting reduces and the higher energy component in the spectrum weakens. At $\theta = 0.59$ the higher energy component appears as a shoulder on one side of the larger peak. Thus, it is

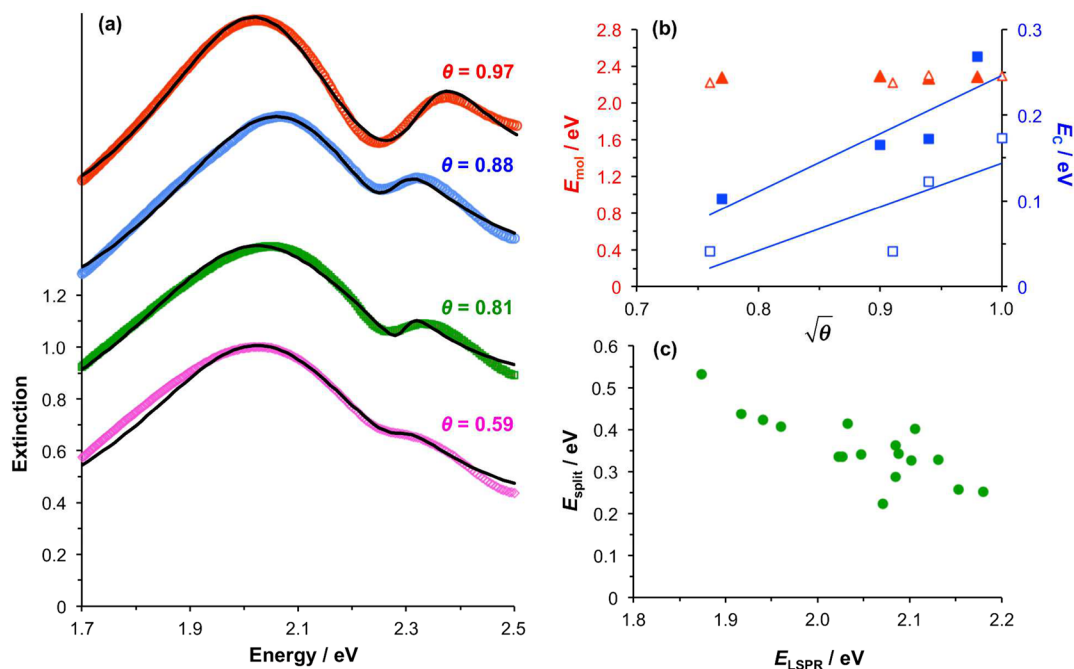


Figure 3. (a) Normalized extinction spectra acquired for an array of gold nanostructures at WT LH2 fractional coverages of 0.59, 0.81, 0.88, and 0.97. (b) Variation in the exciton energy E_{mol} (triangles) and coupling energy E_c (squares) obtained from model fits to the experimental data, as a function of the square root of the fractional coverage for the spectra shown in (a) (solid symbols) and for a second array of nanostructures ($\lambda_{SLR} = 592$ nm, 2.10 eV) treated in a similar fashion (open symbols). The straight lines are guides to the eye. (c) Variation in the experimentally observed splitting energy E_{split} , defined as the distance between the peaks in the extinction spectrum, after attachment of LH2 to arrays of gold nanostructures as a function of the LSPR energy of the clean array.

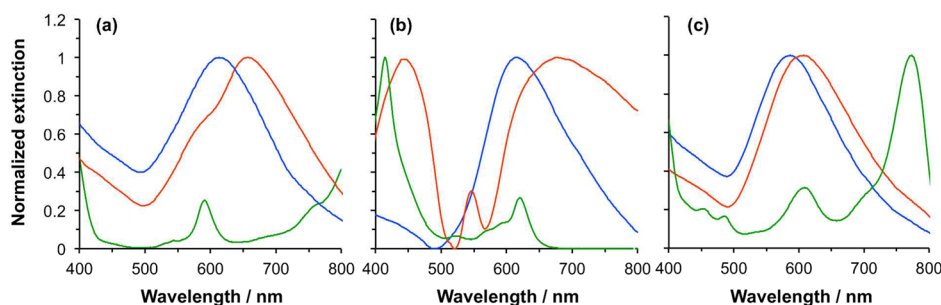


Figure 4. (a) Normalized extinction spectrum of a gold nanostructure array before (blue) and after (light red) (a) attachment of Crt-free LH1; (b) attachment of chlorin-binding His-tagged self-assembled polypeptide maquettes; and (c) adsorption of a monolayer of BChl *a*. The solution-phase absorption spectrum of the each molecule in solution is shown in green.

clear that the splitting varies with the density of dipoles at the surface as expected in strong coupling.

The type of splitting observed in Figures 1–3 is suggestive of an asymmetric resonance where one of the oscillators has a broad line width and the other is narrow, typically leading to Fano-type lineshapes of the coupled system. The system was modeled as two coupled harmonic oscillators yielding an expression for the extinction (see Supporting Information for details), enabling us to model the spectra (Figure 3a). A good fit is observed between the calculated spectra and the experimental data. When the model was applied to the data in Figures 1 and 2 a similarly good fit was obtained (fitted spectra are shown in the Supporting Information).

In the coupled oscillator model the coupling constant g has the dimension of frequency squared (energy squared in a scaled version, denoted G). At resonance when the two oscillators have the same frequency ω , the splitting between the normal modes is approximately g/ω .⁴⁰ To connect to microscopic quantum and semiclassical models of strong coupling, we give here the coupling energy in the form $E_C = G/E_{\text{LSPR}}$ where G is the coupling constant obtained by the fits. The coupling energy was obtained for the systems shown in Figure 3a and for a second, similar system (the cleaning protocol, using piranha solution, does not permit indefinite reuse of the same array so obtaining multiple repeat measurements at different coverages with the same sample is difficult). The data are shown as a function of $\sqrt{\theta}$ in Figure 3b. Descriptions of strong coupling predict⁴⁰ that the coupling energy should be proportional to the square root of the density of dipoles. The data in Figure 3b suggest that this is the case.

A fundamental criterion for strong coupling (see, for instance, ref 40 or the discussion in Supporting Information) is that the coupling energy is similar to or larger than $(\gamma_p - \gamma_{\text{mol}})/2$, where γ_p and γ_{mol} are the line widths of the plasmon mode and the exciton. In Figure 3a, $(\gamma_p - \gamma_{\text{mol}})/2 = 0.21$ eV, and at $\theta = 0.97$, the coupling energy $E_C = 0.27$ eV, satisfying the criterion. However, as θ decreases, E_C falls, reaching 0.17 eV at $\theta = 0.88$. Strictly, therefore, the system only approaches strong coupling at lower coverages. For the spectra in Figure 1, E_C is similar in magnitude to $(\gamma_p - \gamma_{\text{mol}})/2$, as it is for the ΔcrtC mutant of LH1 (Figure 2a). However, for the $\Delta\text{crtI}::\text{crtI}^{\text{Pa}}$ $\Delta\text{crtD}^{\text{Ga}}$ mutant of LH1 (Figure 2b), E_C falls to 0.11 eV, compared to $(\gamma_p - \gamma_{\text{mol}})/2 = 0.23$ eV; for this protein strong coupling is not strictly observed, therefore, consistent with the weaker splitting in the spectrum. Broadly, spectra that exhibited pronounced splitting yielded coupling energies that satisfied the criterion $E_C \geq (\gamma_p - \gamma_{\text{mol}})/2$, but for low coverages of protein,

and for the $\Delta\text{crtI}::\text{crtI}^{\text{Pa}}$ $\Delta\text{crtD}^{\text{Ga}}$ mutant, the coupling was weaker.

The experimentally measured splitting energy E_{split} , defined as the separation of the peaks in the extinction spectrum, is shown in Figure 3c as a function of the LSPR energy for the clean gold array, E_{LSPR} . As expected, E_{split} increases when the separation in energy between the LSPRs and the excitons in LH2 to which they are coupled increases; based on theory, the splitting depends both on the coupling energy and the energy separation between the LSPR and the exciton. The exciton energy E_{mol} was calculated using the coupled harmonic oscillator model for these samples and was found not to vary with E_{LSPR} , as expected from theory. A mean value of $E_{\text{mol}} = 2.27 \pm 0.03$ eV was determined for the 17 samples for which data are shown in Figure 3c, close to the energy of the spheroidenone S2 state in LH2, reported by Cong et al. to be 2.21 eV in LH2.⁶⁰

It is essential to estimate whether the obtained coupling energies can be expected based on microscopic quantities such as the protein (dipole) densities and LSPR mode volumes. We used a microscopic expression^{52,63} for the coupling energy (see Supporting Information). From the parameters determined by modeling of the spectra, we calculated the effective height of the LSPR mode volume on top of the nanostructure. For different coupling energies, we obtained values in the range 1–35 nm, which are realistic although the largest obtained couplings (smallest heights) indicate that hot spots due to nanostructure and metal imperfections⁶⁴ might play a role.

While the transition dipole moment associated with the Q_x transition is an order of magnitude smaller than that associated with the S2 transition in Crt, it is nevertheless possible that there could be strong LSPR- Q_x coupling. To examine this possibility, an array of gold nanostructures was functionalized with a mutant of LH1 that does not contain carotenoids. Figure 4a shows extinction spectra of the array before and after attachment of the protein. Splitting of the plasmon band is observed, but the coupling energy is smaller than is observed in Figures 2 and 3; the high-energy component in the spectrum appears as a shoulder on the larger low-energy resonance, similar to the case for $\theta = 0.59$ in Figure 3a.

Comparative spectra were acquired for self-assembling peptide “maquettes”.^{65,66} Maquettes are synthetic 4- α -helical proteins in which specific biological function is designed *ab initio* by the selection of amino acid sequences that will fold to present functional units in desired configurations. In previous studies, maquette structures have been designed that have matched the oxygen-transferring capacity of myoglobin.⁶⁷ More recently, sequences have been described that incorporate

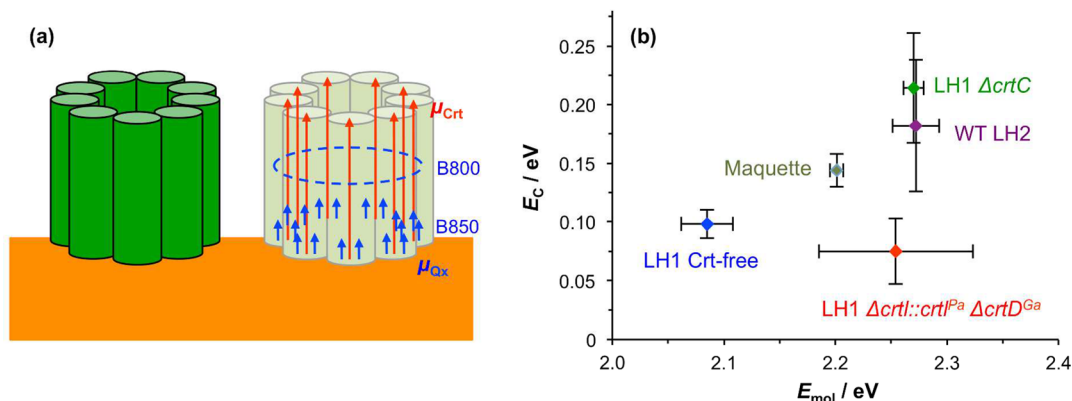


Figure 5. (a) Schematic diagram showing His-tagged LH2 on a gold nanostructure (left) and the Crt and B850 Q_x transition dipoles (right), after Cogdell et al.⁷¹ A further nine Q_x dipoles lie in the B800 ring, oriented parallel to the plane of the gold surface (dashed blue ring). (b) Variation in the coupling energy with the exciton energy for the systems studied here.

haem-binding tetrapyrrole structures that have exhibited oxidoreductive activities.⁶⁸ In the present study, a maquette was designed that incorporated a synthetic SE369 chlorin⁶⁹ and a histidine tag for surface attachment, but no carotenoids. SE369 is a member of the family of de novo synthesized chlorins that bear a geminal-dimethyl group to impart stability.⁷⁰ Significant changes are observed in the extinction spectrum after attachment of maquettes to an array of gold nanostructures (Figure 4b). The solution-phase spectrum of the maquettes exhibits a peak at 620 nm. This feature is close in energy to the LSPR, at 615 nm, which is split after coupling of the maquettes to the array to yield two components at 548 and 675 nm. The similarity between the Au-maquette spectrum and the extinction spectra of arrays functionalized by LH1 and LH2 is striking, indicative that LSPRs are also strongly coupled to the chlorins in these synthetic proteins.

Measurements were made of the extinction spectra of arrays of gold nanostructures after deposition of BChl *a* by physisorption from solution (Figure 4c). The spectrum now consists of a single peak at 596 nm, corresponding to a red-shifted plasmon band. The magnitude of the shift is 9 nm, indicating that a significant amount of BChl was adsorbed at the surface. However, there is no evidence of splitting of the plasmon band. This observation is surprising, given the similar dipole strengths. The surface density of dipoles is expected to influence the strength of plasmon exciton coupling. For a flat-lying monolayer of BChl, based on its known dimensions, a density of ca. $8 \times 10^{17} \text{ m}^{-2}$ is estimated; for molecules aligned perpendicular to the surface plane the density would be higher. However, for LH2, the density of BChl is estimated to be ca. $4.2 \times 10^{17} \text{ m}^{-2}$ (see Supporting Information for justification). Based on these considerations there seems to be no reason to predict a reduced strength of plasmon–exciton coupling for BChl.

If differences in the density of dipoles cannot explain the observation of splitting in the extinction spectra of arrays functionalized with light-harvesting complexes and maquettes, but not of arrays covered with BChl, then the explanation must lie in the presentation of the pigment molecules within the plasmon mode volume: the observation of strong plasmon–exciton coupling requires not simply gold nanostructures and the presence of BChl and Crt within the LSPR mode volume. Rather, strong coupling requires a particular presentation of pigments that must be ideal in light harvesting complexes (Figure 5a).

Figure 5b shows the coupling energy as a function of E_{mol} for all of the systems studied here. Both values are extracted from the experimental spectra using the coupled harmonic oscillator model. The smallest exciton energy, 2.09 eV, was calculated for the Crt-free mutant of LH1. For this protein, the plasmon couples to the Q_x state in the BChl. The solution-phase spectrum of this protein yields an energy of 2.11 eV for this transition, close to the extracted value. In general, the coupling strength increases as the exciton energy increases, as expected based on microscopic theory.⁴⁰ Variation is also expected due to different dipole moments of the different systems. The coupling is notably stronger for the maquettes than for the Crt-free LH1, which is significant given that in both cases the pigment is a chlorin. It is possible that the conformation of the maquette presents the chlorins in such a way that there is reinforcement of the effective dipole moment (the chlorins are expected to be approximately collinear). The largest coupling (0.21 eV) is observed for the $\Delta crtC$ mutant of LH1, which yields the highest energy Crt S2 transition among the molecules studied here (Figure 2d). However, WT LH2 also yields a very large coupling strength (0.18 eV). The $\Delta crtI::crtI^{Pa} \Delta crtD^{Ga}$ mutant yields the smallest coupling strength (0.08 eV). The reasons for this are not clear, although an explanation may lie in the fact that this protein contains a mixture of carotenoids.

The differences thus observed in strong coupling must reflect different organization and coupling of the chromophores within the proteins, giving new dimensions of analysis to how they operate to transfer optical energy into the reaction centers that they feed.

In conclusion, surface plasmon resonances (LSPR) of gold nanostructures in macroscopically extended, periodic arrays are strongly coupled to excitons in the pigment molecules in light-harvesting complexes 1 and 2 from *R. sphaeroides* and chlorin-containing man-made 4- α -helical maquette proteins. This coupling leads to a substantial splitting of the plasmon band and the observation of significant changes in the extinction spectrum. The plasmon–exciton coupling is modeled with two coupled harmonic oscillators and provides a very good fit to the experimental data, enabling the extraction of the exciton energies. For wild type LH2 this is estimated to be 2.27 ± 0.03 eV, close to the energy of the S2 state in spheroidenone. Coupling energies are found to be in the range 0.1–0.2 eV depending on the type of light-harvesting complex and its pigment composition. Consistent with expectations for strong plasmon–exciton coupling, significant changes are observed in

extinction spectra as a function of protein surface coverage. The coupling energy is found to vary with the square root of the coverage. Strong coupling is not observed for bacteriochlorophyll *a*, however. It is hypothesized that strong coupling requires a particular presentation of the pigment molecules. Specifically, this must be the presentation found in light harvesting complexes. A possible explanation is that strong coupling results from coherent coupling of the LSPR to an electronically coherent array of excitons. Studies of such strongly coupled systems may thus yield insights into energy transfer pathways in photosynthesis.

■ ASSOCIATED CONTENT

Supporting Information

The Supporting Information is available free of charge on the ACS Publications website at DOI: [10.1021/acs.nanolett.6b02661](https://doi.org/10.1021/acs.nanolett.6b02661).

Further details of the experimental and theoretical methods (PDF)

■ AUTHOR INFORMATION

Corresponding Authors

*E-mail: graham.leggett@sheffield.ac.uk.

*E-mail: paivi.torma@aalto.fi.

Notes

The authors declare no competing financial interest.

■ ACKNOWLEDGMENTS

The authors are grateful to EPSRC (grants EP/I012060/1, EP/G060649/1, EP/L027151/1, and EP/K028510/1) for Financial Support. Prof J. S. Lindsey, North Carolina State University, is thanked for providing support for O.A.M. during the preparation of synthetic chlorin SE369. This research was carried out as part of the Photosynthetic Antenna Research Center (PARC), an Energy Frontier Research Center funded by the U.S. Department of Energy, Office of Science, Office of Basic Energy Sciences, under Award DESC0001035 supporting G.K. and P.L.D. in light harvesting maquette construction and characterization. This work was supported by the Academy of Finland through its Centres of Excellence Programme (2012-2017) and under project Nos. 263347, 284621, and 272490 and by the European Research Council (ERC-2013-AdG-340748-CODE (to P.T.) and Advanced Award 338895 (to C.N.H.) and award LINASS 320503 (to J. J. B)). The SYNECO project collaboration is acknowledged. C.N.H. gratefully acknowledges financial support from the Biotechnology and Biological Sciences Research Council (BBSRC UK), award number BB/G021546/1.

■ REFERENCES

- (1) Blankenship, R. E. *Molecular Mechanisms of Photosynthesis*, 2nd ed.; Wiley-Blackwell: Chichester, 2014.
- (2) Sener, M. K.; Olsen, J. D.; Hunter, C. N.; Schulten, K. *Proc. Natl. Acad. Sci. U. S. A.* **2007**, *104*, 15723.
- (3) Cartron, M. L.; Olsen, J. D.; Sener, M.; Jackson, P. J.; Brindley, A. A.; Qian, P.; Dickman, M. J.; Leggett, G. J.; Schulten, K.; Hunter, C. N. *Biochim. Biophys. Acta, Bioenerg.* **2014**, *1837*, 1769.
- (4) Şener, M.; Strümpfer, J.; Hsin, J.; Chandler, D.; Scheuring, S.; Hunter, C. N.; Schulten, K. *ChemPhysChem* **2011**, *12*, 518.
- (5) Fleming, G. R.; Schlau-Cohen, G. S.; Amarnath, K.; Zaks, J. *Faraday Discuss.* **2012**, *155*, 27.
- (6) McGlynn, P.; Westerhuis, W. H. J.; Jones, M. R.; Hunter, C. N. *J. Biol. Chem.* **1996**, *271*, 3285.

- (7) Cogdell, R. J.; Isaacs, N. W.; Howard, T. D.; McLuskey, K.; Fraser, N. J.; Prince, S. M. *J. Bacteriol.* **1999**, *181*, 3869.
- (8) Cory, M. G.; Zerner, M. C.; Hu, X.; Schulten, K. *J. Phys. Chem. B* **1998**, *102*, 7640.
- (9) Lee, H.; Cheng, Y.-C.; Fleming, G. R. *Science* **2007**, *316*, 1462.
- (10) Ishizaki, A.; Fleming, G. R. *New J. Phys.* **2010**, *12*, 055004.
- (11) Ryu, I. S.; Dong, H.; Fleming, G. R. *J. Phys. Chem. B* **2014**, *118*, 1381.
- (12) Engel, G. S.; Calhoun, T. R.; Read, E. L.; Ahn, T.-K.; Mancal, T.; Cheng, Y.-C.; Blankenship, R. E.; Fleming, G. R. *Nature* **2007**, *446*, 782.
- (13) Hildner, R.; Brinks, D.; Nieder, J. B.; Cogdell, R. J.; van Hulst, N. F. *Science* **2013**, *340*, 1448.
- (14) Collini, E.; Wong, C. Y.; Wilk, K. E.; Curmi, P. M. G.; Brumer, P.; Scholes, G. D. *Nature* **2010**, *463*, 644.
- (15) Dahlberg, P. D.; Norris, G. J.; Wang, C.; Viswanathan, S.; Singh, V. P.; Engel, G. S. *J. Chem. Phys.* **2015**, *143*, 101101.
- (16) Maier, S. A.; Brongersma, M. L.; Kik, P. G.; Meltzer, S.; Requicha, A. A. G.; Atwater, H. A. *Adv. Mater.* **2001**, *13*, 1501.
- (17) Barnes, W. L.; Dereux, A.; Ebbesen, T. W. *Nature* **2003**, *424*, 824.
- (18) Gray, S. K. *J. Phys. Chem. C* **2012**, *117*, 1983.
- (19) Ergin, T.; Stenger, N.; Brenner, P.; Pendry, J. B.; Wegener, M. *Science* **2010**, *328*, 337.
- (20) Fang, N.; Lee, H.; Sun, C.; Zhang, Xi. *Science* **2005**, *308*, 534.
- (21) Hibbins, A. P.; Evans, B. R.; Sambles, J. R. *Science* **2005**, *308*, 670.
- (22) Ebbesen, T. W.; Lezec, H. J.; Ghaemi, H. F.; Thio, T.; Wolff, P. A. *Nature* **1998**, *391*, 667.
- (23) Anker, J. N.; Hall, W. P.; Lyandres, O.; Shah, N. C.; Zhao, J.; Van Duyne, R. P. *Nat. Mater.* **2008**, *7*, 442.
- (24) Prodan, E.; Radloff, C.; Halas, N. J.; Nordlander, P. *Science* **2003**, *302*, 419.
- (25) Martin, J.; Kociak, M.; Mahfoud, Z.; Proust, J.; Gérard, D.; Plain, J. *Nano Lett.* **2014**, *14*, 5517.
- (26) Olson, J.; Manjavacas, A.; Liu, L.; Chang, W.-S.; Foerster, B.; King, N. S.; Knight, M. W.; Nordlander, P.; Halas, N. J.; Link, S. *Proc. Natl. Acad. Sci. U. S. A.* **2014**, *111*, 14348.
- (27) Rosi, N. L.; Mirkin, C. A. *Chem. Rev.* **2005**, *105*, 1547.
- (28) Elghanian, R.; Storhoff, J. J.; Mucic, R. C.; Letsinger, R. L.; Mirkin, C. A. *Science* **1997**, *277*, 1078.
- (29) Valsecchi, C.; Brolo, A. G. *Langmuir* **2013**, *29*, 5638.
- (30) Lee, S.-W.; Lee, K.-S.; Ahn, J.; Lee, J.-J.; Kim, M.-G.; Shin, Y.-B. *ACS Nano* **2011**, *5*, 897.
- (31) Nie, S.; Emory, S. R. *Science* **1997**, *275*, 1102.
- (32) Chen, S.-Y.; Mock, J. J.; Hill, R. T.; Chilkoti, A.; Smith, D. R.; Lazarides, A. A. *ACS Nano* **2010**, *4*, 6535.
- (33) Chen, S.; Svedendahl, M.; Antosiewicz, T. J.; Kall, M. *ACS Nano* **2013**, *7*, 8824.
- (34) Langguth, L.; Punj, D.; Wenger, J. R. M.; Koenderink, A. F. *ACS Nano* **2013**, *7*, 8840.
- (35) Ahijado-Guzmán, R.; Prasad, J.; Rosman, C.; Henkel, A.; Tome, L.; Schneider, D.; Rivas, G.; Sönnichsen, C. *Nano Lett.* **2014**, *14*, 5528.
- (36) Bujak, Å.; Czechowski, N.; Piatkowski, D.; Litvin, R.; Mackowski, S.; Brotosudarmo, T. H. P.; Cogdell, R. J.; Pichler, S.; Heiss, W. *Appl. Phys. Lett.* **2011**, *99*, 173701.
- (37) Bujak, L.; Olejnik, M.; Brotosudarmo, T. H. P.; Schmidt, M. K.; Czechowski, N.; Piatkowski, D.; Aizpurua, J.; Cogdell, R. J.; Heiss, W.; Mackowski, S. *Phys. Chem. Chem. Phys.* **2014**, *16*, 9015.
- (38) Brecht, M.; Hussels, M.; Nieder, J. B.; Fang, H.; Elsässer, C. *Chem. Phys.* **2012**, *406*, 15.
- (39) Nieder, J. B.; Bittl, R.; Brecht, M. *Angew. Chem., Int. Ed.* **2010**, *49*, 10217.
- (40) Törmä, P.; Barnes, W. L. *Rep. Prog. Phys.* **2015**, *78*, 013901.
- (41) González-Tudela, A.; Huidobro, P. A.; Martín-Moreno, L.; Tejedor, C.; García-Vidal, F. J. *Phys. Rev. Lett.* **2013**, *110*, 126801.
- (42) Bellessa, J.; Bonnand, C.; Plenet, J. C.; Mugnier, J. *Phys. Rev. Lett.* **2004**, *93*, 036404.

- (43) Dintinger, J.; Klein, S.; Bustos, F.; Barnes, W. L.; Ebbesen, T. W. *Phys. Rev. B: Condens. Matter Mater. Phys.* **2005**, *71*, 035424.
- (44) Sugawara, Y.; Kelf, T. A.; Baumberg, J. J.; Abdelsalam, M. E.; Bartlett, P. N. *Phys. Rev. Lett.* **2006**, *97*, 266808.
- (45) Wurtz, G. A.; Evans, P. R.; Hendren, W.; Atkinson, R.; Dickson, W.; Pollard, R. J.; Zayats, A. V.; Harrison, W.; Bower, C. *Nano Lett.* **2007**, *7*, 1297.
- (46) Fofang, N. T.; Park, T.-H.; Neumann, O.; Mirin, N. A.; Nordlander, P.; Halas, N. J. *Nano Lett.* **2008**, *8*, 3481.
- (47) Vasa, P.; Wang, W.; Pomraenke, R.; Lammers, M.; Maiuri, M.; Manzoni, C.; Cerullo, G.; Lienau, C. *Nat. Photonics* **2013**, *7*, 128.
- (48) Zengin, G.; Wersäll, M.; Nilsson, S.; Antosiewicz, T. J.; Käll, M.; Shegai, T. *Phys. Rev. Lett.* **2015**, *114*, 157401.
- (49) Fales, A. M.; Norton, S. J.; Crawford, B. M.; DeLacy, B. G.; Vo-Dinh, T. *Phys. Chem. Chem. Phys.* **2015**, *17*, 24931.
- (50) DeLacy, B. G.; Miller, O. D.; Hsu, C. W.; Zander, Z.; Lacey, S.; Yagloski, R.; Fountain, A. W.; Valdes, E.; Anquillare, E.; Soljačić, M.; Johnson, S. G.; Joannopoulos, J. D. *Nano Lett.* **2015**, *15*, 2588.
- (51) Hakala, T. K.; Toppari, J. J.; Kuzyk, A.; Pettersson, M.; Tikkanen, H.; Kunttu, H.; Törmä, P. *Phys. Rev. Lett.* **2009**, *103*, 053602.
- (52) Shi, L.; Hakala, T. K.; Rekola, H. T.; Martikainen, J. P.; Moerland, R. J.; Törmä, P. *Phys. Rev. Lett.* **2014**, *112*, 153002.
- (53) Väkeväinen, A. I.; Moerland, R. J.; Rekola, H. T.; Eskelinen, A. P.; Martikainen, J. P.; Kim, D. H.; Törmä, P. *Nano Lett.* **2014**, *14*, 1721.
- (54) Luk'yanchuk, B.; Zheludev, N. I.; Maier, S. A.; Halas, N. J.; Nordlander, P.; Giessen, H.; Chong, C. T. *Nat. Mater.* **2010**, *9*, 707.
- (55) Wu, C.; Khanikaev, A. B.; Adato, R.; Arju, N.; Yanik, A. A.; Altug, H.; Shvets, G. *Nat. Mater.* **2012**, *11*, 69.
- (56) Gallinet, B.; Martin, O. J. F. *Phys. Rev. B: Condens. Matter Mater. Phys.* **2011**, *83*, 235427.
- (57) Auguie, B.; Barnes, W. *Phys. Rev. Lett.* **2008**, *101*, 143902.
- (58) Rodriguez, S. R. K.; Rivas, J. G. *Opt. Express* **2013**, *21*, 27411.
- (59) Tsargorodska, A.; El Zubir, O.; Darroch, B.; Cartron, M. L.; Basova, T.; Hunter, C. N.; Nabok, A. V.; Leggett, G. J. *ACS Nano* **2014**, *8*, 7858.
- (60) Cong, H.; Niedzwiedzki, D. M.; Gibson, G. N.; LaFountain, A. M.; Kelsh, R. M.; Gardiner, A. T.; Cogdell, R. J.; Frank, H. A. *J. Phys. Chem. B* **2008**, *112*, 10689.
- (61) Georgakopoulou, S.; van Grondelle, R.; van der Zwan, G. *Biophys. J.* **2004**, *87*, 3010.
- (62) Chi, S. C.; Mothersole, D. J.; Dilbeck, P.; Niedzwiedzki, D. M.; Zhang, H.; Qian, P.; Vasilev, C.; Grayson, K. J.; Jackson, P. J.; Martin, E. C.; Li, Y.; Holten, D.; Neil Hunter, C. *Biochim. Biophys. Acta, Bioenerg.* **2015**, *1847*, 189.
- (63) Agranovich, V. M.; Litinskaia, M.; Lidzey, D. G. *Phys. Rev. B: Condens. Matter Mater. Phys.* **2003**, *67*, 085311.
- (64) Barbry, M.; Koval, P.; Marchesin, F.; Esteban, R.; Borisov, A. G.; Aizpurua, J.; Sánchez-Portal, D. *Nano Lett.* **2015**, *15*, 3410.
- (65) Farid, T. A.; Kodali, G.; Solomon, L. A.; Lichtenstein, B. R.; Sheehan, M. M.; Fry, B. A.; Bialas, C.; Ennist, N. M.; Siedlecki, J. A.; Zhao, Z.; Stetz, M. A.; Valentine, K. G.; Anderson, J. L. R.; Wand, A. J.; Discher, B. M.; Moser, C. C.; Dutton, P. L. *Nat. Chem. Biol.* **2013**, *9*, 826.
- (66) Koder, R. L.; Dutton, P. L. *Dalton Trans.* **2006**, 3045.
- (67) Koder, R. L.; Anderson, J. L. R.; Solomon, L. A.; Reddy, K. S.; Moser, C. C.; Dutton, P. L. *Nature* **2009**, *458*, 305.
- (68) Solomon, L. A.; Kodali, G.; Moser, C. C.; Dutton, P. L. *J. Am. Chem. Soc.* **2014**, *136*, 3192.
- (69) Aravindu, K.; Mass, O.; Vairaprakash, P.; Springer, J. W.; Yang, E.; Niedzwiedzki, D. M.; Kirmaier, C.; Bocian, D. F.; Holten, D.; Lindsey, J. S. *Chem. Sci.* **2013**, *4*, 3459.
- (70) Lindsey, J. S. *Chem. Rev.* **2015**, *115*, 6534.
- (71) Cogdell, R. J.; Isaacs, N. W.; Freer, A. A.; Howard, T. D.; Gardiner, A. T.; Prince, S. M.; Papiz, M. Z. *FEBS Lett.* **2003**, *555*, 35.